Bioreactor-based bone tissue engineering: The influence of dynamic flow on osteoblast phenotypic expression and matrix mineralization

Xiaojun Yu*, Edward A. Botchwey†, Elliot M. Levine‡, Solomon R. Pollack§, and Cato T. Laurencin*†¶‖

Departments of *Orthopaedic Surgery, †Biomedical Engineering, and ¶Chemical Engineering, University of Virginia, Charlottesville, VA 22903; ‡The Wistar Institute, Philadelphia, PA 19104; and §Department of Bioengineering, University of Pennsylvania, Philadelphia, PA 19104

Edited by Robert S. Langer, Massachusetts Institute of Technology, Cambridge, MA, and approved June 22, 2004 (received for review April 9, 2004)

An important issue in tissue engineering concerns the possibility of limited tissue ingrowth in tissue-engineered constructs because of insufficient nutrient transport. We report a dynamic flow culture system using high-aspect-ratio vessel rotating bioreactors and 3D scaffolds for culturing rat calvarial osteoblast cells. 3D scaffolds were designed by mixing lighter-than-water (density, <1 g/ml) and heavier-than-water (density, >1 g/ml) microspheres of 85:15 poly(lactide-*co*-glycolide). We quantified the rate of 3D flow through the scaffolds by using a particle-tracking system, and the results suggest that motion trajectories and, therefore, the flow velocity around and through scaffolds in rotating bioreactors can be manipulated by varying the ratio of heavier-than-water to lighter-than-water microspheres. When rat primary calvarial cells were cultured on the scaffolds in bioreactors for 7 days, the 3D dynamic flow environment affected bone cell distribution and enhanced cell phenotypic expression and mineralized matrix synthesis within tissue-engineered constructs compared with static conditions. These studies provide a foundation for exploring the effects of dynamic flow on osteoblast function and provide important insight into the design and optimization of 3D scaffolds suitable in bioreactors for *in vitro* tissue engineering of bone.

Bone-grafting surgeries have been widely used by orthopedic surgeons to repair or replace bone damaged or disordered due to trauma, tumor resection, pathological degeneration, and congenital deformity. Approximately 1 million orthopedic surgeries involving the use of bone-grafting materials are performed every year in the United States alone (1, 2). Bone graft materials include autograft, allograft, xenograft, and synthetic materials. An autograft or autogeneous bone is osteoconductive, osteoinductive, and osteogenic, so it sets the gold standard for clinical bone repair (3). However, the application of an autograft is restricted by limited availability and donor-site complications, including infection and chronic pain (4, 5). Allograft or allogenic bone has also been used as a skeletal substitute material. The application of an allograft is also limited by the source of supply and has a risk of transmission of disease, such as HIV and hepatitis B (6). Synthetic bone substitutes, such as synthetic hydroxyapatite and bone cement of hydroxyapatite, have been developed in reconstructive orthopaedic surgery (7, 8). Although synthetic hydroxyapatite has excellent biocompatibility and good osteoconductivity, its clinical applications are limited because of either the difficulty of being resorbed after long-term implantation (9) or low mechanical properties (10).

Because of the limitations associated with biological and synthetic bone grafts, tissue-engineering approaches have been widely studied for the development of bone substitutes. As cells in the body grow in three dimensions anchored onto a network of extracellular matrix (11), a scaffold is needed to recreate the 3D environment. The materials used to make 3D scaffolds for bone tissue engineering include collagen gel matrices (12), porous calcium phosphate-based ceramics (13), degradable PLA, PGA, and their copolymers (14, 15), poly(lactide-*co*-glycolide) (PLAGA) polymer/ceramic composites (16), and degradable polyphosphazenes (17). Biodegradable polyesters, such as polyglycolide, polylactide, and their copolymers, have been extensively used as bone graft substitutes because of their biocompatibility, osteoconductivity, and biodegradability, which in turn eliminates the need for the eventual surgical removal of the scaffold. Deposition of mineralized extracellular matrix by osteoblast cells cultured on porous PLAGA scaffolds has been observed (14–16).

Studies have suggested that the limited diffusion in static culture environments may constrain tissue ingrowth in tissue-engineered constructs. In static cultures, tissue ingrowth was limited to a depth of 200–800 μm in PLAGA foams (14). To overcome the drawbacks associated with static culturing systems, considerable interest has been generated in tissue engineering by using the high-aspect-ratio vessel rotating bioreactor, which has the characteristic of low-shear, three dimensionality and high-mass transfer and thus provides a dynamic flow culture condition to promote tissue synthesis (18–21). Various cell types can form 3D assemblies in the rotating bioreactors (22–26). Rat stromal cells cultured on cytodex-3 beads have been shown to form aggregates and synthesize mineralized matrix, and cell aggregates formed by MC3T3 osteoblast-like cells produced collagen fibrils in the matrix between microspheres (17). When culturing rat bone marrow cells on PLAGA scaffolds in rotating bioreactors, the cells were more uniformly distributed throughout the scaffolds than in static cultures (27).

However, the aggregate densities of conventional scaffolds are usually greater than the surrounding medium in rotating bioreactors, and thus centrifugal force causes the scaffolds to frequently collide with the bioreactor walls during rotation. The collision of the scaffolds with the walls has been shown to be a confounding factor that induces cell damage and disrupts cell attachment and mineralized matrix deposition on the scaffolds (26–28). In addition, the effects of flow-induced shear stresses and mass transfer on cells attached to scaffolds in a rotating bioreactor are complex, and the relationship between the hydrodynamic forces of the rotating bioreactor and cellular response remains elusive (29).

Building on past accomplishments, we have adopted a dynamic flow culture system that makes use of 3D degradable microcarrier scaffolds and the high-aspect-ratio vessel rotating bioreactor for *in vitro* osteoblast culture and bone tissue engineering (30, 31). In previous studies, we described the development of PLAGA (50:50) hollow microsphere-based 3D lighter-than-water (LTW) scaffolds that have densities less than the

This paper was submitted directly (Track II) to the PNAS office.

Abbreviations: PLAGA, poly(lactide-*co*-glycolide); LTW, lighter than water; HTW, heavier than water; MTT, 3-(4,5-dimethylthiazol-2-yl)-2,5-diphenyl tetrazolium bromide; SEM, scanning electronic microscope.

‖To whom correspondence should be addressed at: Department of Orthopaedic Surgery, University of Virginia, 400 Ray C. Hunt Drive, Suite 330, Charlottesville, VA 22903. E-mail: ctl3f@virginia.edu.

media (1 g/ml). These scaffolds have trajectories that facilitate media perfusion in the rotating bioreactors. As a result, differentiation and mineralization of human osteoblastic cells (Saos-2) seeded on these scaffolds were significantly enhanced (30). In addition, we have also created "mixed" density scaffolds by combining heavier-than-water (HTW) and LTW microspheres.

In this study, we further characterize the movement of mixed scaffolds of PLAGA (85:15) in high-aspect-ratio vessel rotating bioreactors and seek to determine the effects of dynamic-flow-induced nutrient transport on *in vitro* cell proliferation, cell differentiation, mineralized matrix synthesis, and expression of selected bone marker proteins of rat primary calvarial osteoblastic cells cultured on the mixed scaffolds in rotating bioreactors *in vitro*.

Materials and Methods

Microsphere Preparation. LTW and HTW biodegradable polymeric microspheres were fabricated with PLAGA copolymer in an 85:15 ratio (Alkermes Medisorb, Wilmington, OH) as described (30, 32). The polymer was amorphous and had an inherent viscosity of 0.66–0.80 dl/g and a glass transition temperature of 50–55°C. In brief, PLAGA was dissolved in methylene chloride (Aldrich) at 30% (wt/v), and 10% (vol/vol) of distilled water was added into the solution to generate bubbles. The solution was slowly poured into a 0.1% (wt/vol) polyvinyl alcohol (molecular mass = 30,000–70,000 Da; Sigma) solution stirring at 1,500 rpm, and the solvent was allowed to evaporate overnight at room temperature. The LTW (present at surface of the solution) and HTW (present at bottom of the solution) microspheres were collected separately and washed extensively with distilled water to remove the remaining solvent and polyvinyl alcohol. The microspheres were freeze-dried by using a lyophilizer (Labconco, Kansas City, MO) overnight. The LTW and HTW biodegradable polymeric microspheres were sieved into different sizes, and microspheres with diameters from 425 to 500 μm were used to fabricate the scaffolds.

Scaffold Preparation and Characterization. The 3D microsphere scaffolds were fabricated into 4 × 2.5 mm (diameter × height) cylindrical scaffolds of varying density by using sintered microsphere methods described (30, 32). In brief, the LTW scaffolds were fabricated by sintering LTW polymeric microspheres of PLAGA at 80°C for 3 h. Different types of mixed microsphere scaffolds were fabricated by sintering the HTW and LTW microspheres in the ratios (wt/wt) of 80:20, 60:40, 40:60, and 20:80 at 80°C for 3 h.

Scaffold Motion Analysis. The movement of scaffolds was tracked by using a real-time visualization unit designed by us (33). In brief, the scaffold-tracking system comprises a charge-coupled device camera (Cohu, San Diego) that is rotated in synchrony with a rotating bioreactor. Scaffold motion was recorded digitally with a video cassette recorder (Sony SVO-9500-MD) and analyzed by using IMAGE PRO (Phase 3 Imaging, Glen Mills, PA). Scaffolds were visualized in a bioreactor rotating at 36 rpm with the real-time visualization unit, and the instantaneous velocity values of the scaffolds were calculated by dividing the distance traveled by the scaffold by the time interval between frames.

By assuming uniform flow past a single microsphere on the surface of the scaffold, the velocity could be used to estimate the maximum fluid shear stress by using the Stokes equation (30)

$$\sigma = \frac{-3\mu U}{2a},$$

where σ is shear stress, μ is viscosity, U is flow velocity, and a is the diameter of the microsphere.

Cell Culture. Rat calvarial osteoblastic cells were isolated from 2-day-old neonatal Sprague–Dawley rats by the enzymatic digestive method and maintained to passage 3 for experiments. One composition of the mixed scaffolds (HTW and LTW microspheres in a ratio of 60:40) was used in the cell culture for comparing dynamic flow and static culture conditions on osteoblastic cells. Scaffolds were sterilized under UV light for 45 min, followed by 70% ethanol for 20 min, and washed with PBS (GIBCO/BRL) twice for 15 min. Cells were seeded onto microsphere scaffolds at a density of 2×10^4 cells per ml for 24 h as described (30). After 24 h (day 0), scaffolds were transferred to 50-ml high-aspect-ratio vessel vessels (Synthecon, Houston) either maintained statically as controls or rotated at 36 rpm as rotating bioreactors. The cells were cultured in Hanks' F-12 media supplemented with 15% FBS (GIBCO/BRL), 1% penicillin/streptomycin (GIBCO/BRL), 1% glucose (Sigma), and 1% β-glycerophosphate (Sigma) at 37°C and 5% CO_2. The media were changed every 3 days, and the cultures were maintained for 7 days. At days 4 and 7, scaffolds were removed and characterized for cell proliferation, differentiation, mineralized matrix synthesis, bone marker protein expression, and morphological analysis.

Cell Proliferation. Cell proliferation was analyzed by using 3-(4,5-dimethylthiazol-2-yl)-2,5-diphenyl tetrazolium bromide (MTT; Sigma) mitochondrial reduction (34). This assay is based on the ability of live cells to reduce a tetrazolium-based compound, MTT, to a purplish formazan product. In brief, scaffolds were washed with PBS, transferred into new Petri dishes containing 0.5 ml of culture medium, and 50 μl of MTT solution (5 mg/ml in PBS) and incubated for 2 h at 37°C. After removing the culture media, 0.5 ml of extraction solution (0.01 N HCl in isopropyl alcohol) was added. The scaffolds were washed extensively by pipetting up and down repeatedly to allow total color release. The absorbance of the supernatant was read with a spectrophotometer at 570 nm. Cell number was determined through a standard curve that was established by using a known number of cells counted by a Coulter counter.

Alkaline Phosphatase Activity. The retention of osteoblastic phenotype at days 4 and 7 was evaluated by measuring alkaline phosphatase activity. The colorimetric method was based on the conversion of *p*-nitrophenyl phosphate into *p*-nitrophenol in the presence of alkaline phosphatase. In brief, the solutions were collected and stored at −70°C freezer. On thawing, a volume of 100-μl sample was added to 1 ml of *p*-nitrophenyl phosphate solution (16 mM; Diagnostic Kit 245, Sigma) at 37°C for 30 min. The production of *p*-nitrophenol was determined by measuring the absorbance with a microplate reader (Shimadzu) at 415 nm. The results for alkaline phosphatase activity were normalized by the number of cells in the scaffolds.

Alizarin Red Calcium Quantification. Mineralized matrix synthesis was analyzed with Alizarin Red staining method for calcium deposition (30). This technique used a colorimetric analysis based on solubilizing the red matrix precipitate with cetylpyridinium chloride to yield a purple solution. In brief, scaffolds were fixed with 70% ethanol at 4°C for 1 h and then stained with 10% Alizarin Red (Sigma) solution for 10 min. After washing five times with distilled water, the red matrix precipitate was solubilized in 10% cetylpyridinium chloride (Sigma), and the optical density of the solution was read at 562 nm with a spectrophotometer (Shimadzu). The calcium deposition was expressed as molar equivalent of $CaCl_2$ and normalized by the average number of cells per scaffold as determined in companion proliferation studies.

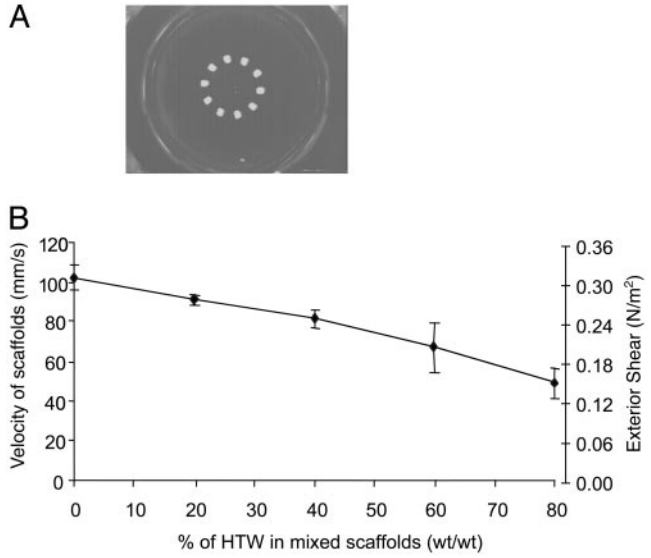

Fig. 1. Scaffold motion tracking. (*A*) Motion trajectories of mixed scaffold with HTW to LTW ratio of 60:40. (*B*) Velocity and shear of scaffolds with various ratios of HTW to LTW ($n = 3$). Error bars denote standard deviation.

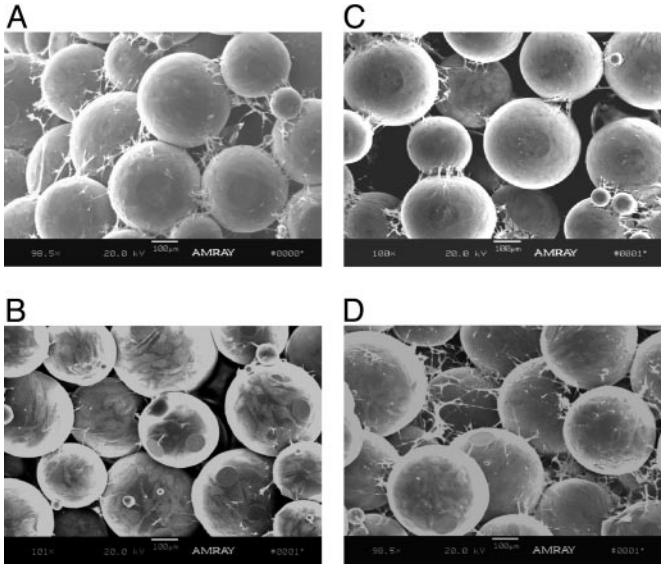

Fig. 2. SEM images. SEM images of rat calvarial cells cultured on the surface (*A* and *C*) and interior (*B* and *D*) of PLAGA scaffolds under static (*A* and *B*) and rotating conditions (*C* and *D*) for 7 days.

Scanning Electron Microscopy. The morphology of cells on scaffolds was observed by using a scanning electronic microscope (SEM; 1830-D4, Amray, Bedford, MA). To observe the interior of the scaffolds, the scaffolds were sectioned in the middle with a razor blade. Scaffolds were fixed in 3% gluteraldehyde at 4°C for 24 h and dried with increasing concentration of ethanol (10, 30, 50, 70, 90, 95, and 100%). Electron microscopy samples were coated with gold by using a Denton Desk-1 Sputter coater. Surfaces were visualized at an accelerating voltage of 20 kv by using an Amray 1830-D4 equipped with a tungsten electron gun.

Osteocalcin and Osteopontin Expression: ELISA. The expression of osteocalcin and osteopontin was analyzed by ELISA. In brief, the scaffolds with cells were lysed with 0.1% Triton X-100 (Sigma). The protein amount was estimated by Bio-Rad protein assay. Four micrograms of protein were added into each well of a 96-well plate at room temperature for 1 h. Twenty microliters of goat anti-rat antibodies against osteocalcin (Diagnostic Systems Laboratories, Webster, TX) or rabbit anti-rat antibodies against osteopontin (Assay Designs, Ann Arbor, MI) were added to the wells separately at 1:100 and incubated at 4°C overnight. After washing with PBS, 20 μl of alkaline phosphatase-conjugated mouse anti-goat (or mouse anti-rabbit) secondary antibody (Santa Cruz Biotechnology) (1:100) was added into each well and incubated at 4°C overnight. After washing with PBS, 100 μl of substrates *p*-nitro blue tetrazolium chloride (0.734 mmol/liter; Sigma) and 5-bromo-4-chloro-3 indolyl-phosphate (0.692 mmol/liter; Sigma) were added into each well and incubated at room temperature for 2 h. The absorbance of the supernatant was read at 620 nm by using a plate reader (TECAN, Crailsheim, Germany).

Statistical Analysis. A two-tailed Student's *t* test was used for comparing the results between the static and rotated groups. A *P* value of <0.05 was considered to be statistically significant.

Results

Scaffold Motion Analysis. The scaffold trajectories are shown in Fig. 1*A*. The aggregate densities of the LTW scaffolds and the mixed scaffolds (HTW/LTW, 60:40) are less than the surrounding medium, and the buoyant forces drag the scaffolds toward the center of the bioreactor vessel and keep the scaffolds from collisions with the bioreactor wall (Fig. 1*A*). By varying the ratio of LTW to HTW microspheres in the scaffolds, the velocity values of the scaffolds decreased from 103.1 $\pm$ 6.2 mm/s to 48.9 $\pm$ 7.5 mm/s (Fig. 1*B*). From these velocity measurements and the geometry of the scaffolds (and diameter of isolated microspheres), maximum fluid shear stress was estimated by assuming uniform flow past a single microsphere on the surface of the scaffold and by using the Stokes equation. The estimated maximum shear stress decreased from 0.32 N/m^2 to 0.16 N/m^2 as the ratio of HTW to LTW microspheres changed from 0 to 80% (Fig. 1*B*). Thus, the fluid shear stresses of the scaffolds can be adjusted by varying the ratio of HTW and LTW.

Cell Growth. The cell growth and distribution in the scaffolds was visualized by using SEM. After 7 days of static culture, SEM analysis showed that cells accumulated mainly on the surface of the scaffolds in static culture conditions, whereas cells predominantly occupied the interior of the scaffolds in the rotating bioreactors (Fig. 2). In Fig. 2*A*, cells were clearly visible on the surface of the scaffold, but fewer cells were present within the scaffold interior where nutrients are insufficient to maintain cell viability (Fig. 2*B*). In contrast, osteoblastic cells appeared to completely and preferentially cover the microspheres on the interior of the scaffolds cultured with rotation, and cell ingrowth spans the entire depth of the 2.5-mm structure (Fig. 2 *C* and *D*). Abundant cellular connections appeared in the interior of the scaffolds under rotating conditions (Fig. 2*D*).

Cell Proliferation. The cell proliferation was analyzed by the MTT assay. Based on the MTT assay, no significant difference was observed for cell numbers under rotating conditions compared with static cultures after 4 and 7 days (Fig. 3), indicating that cell proliferation was not affected by dynamic flow conditions for the scaffolds under study.

Alkaline Phosphatase Activity. The phenotypic expressions of cells were evaluated by colorimetric analysis for alkaline phosphatase activity at days 4 and 7. Compared with static conditions, the expression of alkaline phosphatase in cells cultured in rotating bioreactors was significantly enhanced at days 4 and 7 (Fig. 4),

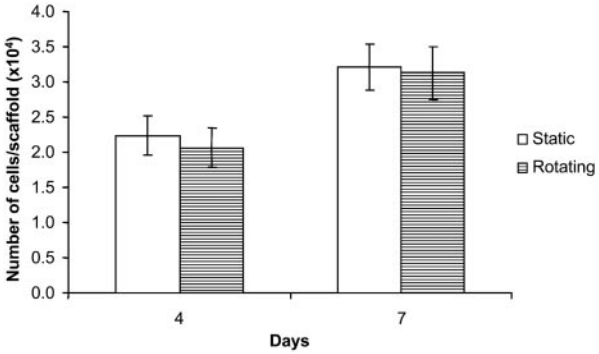

Fig. 3. MTT assay for cell proliferation. At least three scaffolds from each group were analyzed. Error bars denote standard deviation.

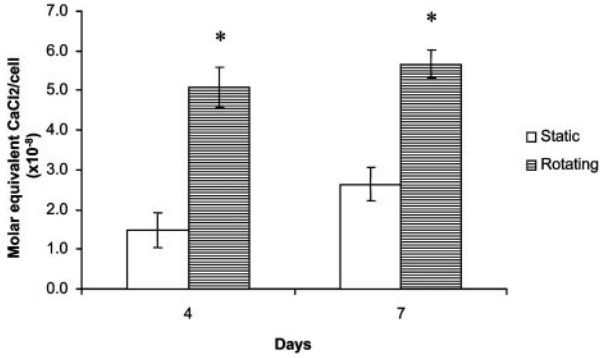

Fig. 5. Alizarin Red assay for calcium deposition. *, A statistically significant, higher ($P < 0.05$) calcium amount than that at static culture conditions. At least three scaffolds from each group were measured. Error bars denote standard deviation.

suggesting that bone cell phenotype expression was stimulated under dynamic flow.

Mineralized Matrix Formation. The production of calcified matrix was analyzed by Alizarin Red histochemical staining. Alizarin Red analysis demonstrated that calcium deposition was significantly increased ($P < 0.05$) after 4 and 7 days in the scaffolds under rotating conditions as compared with those in nonrotating controls (Fig. 5).

Octeocalcin and Osteopontin Expression. The expressions of octeocalcin and osteopontin by the cells on the scaffolds were analyzed by ELISA. Based on the ELISA assay, the levels of osteocalcin and osteopontin were significantly increased ($P < 0.05$) under rotating conditions compared with those in static cultures at days 4 and 7 (Figs. 6 and 7). The results indicated that dynamic flow up-regulated the expression of osteocalcin and osteopontin at both days 4 and 7.

Discussion

Our study addresses fundamental issues facing bone remodeling and formation, in particular, regarding the effects of a dynamic flow in a 3D environment on bone cell biology and bone formation *in vitro*. We are trying to provide important basic information to elucidate the effect of dynamic flow on osteoblast proliferation, phenotype development, and matrix synthesis in a tissue-engineered construct.

Studies have shown that conventional scaffolds (scaffolds with greater aggregate density than the surrounding medium) undergo repeated collisions with the bioreactor wall, imposing a variety of confounding, nonquantifiable mechanical disruptions to cultured cells. These frequent collisions have been shown by our laboratory and others to severely limit achievable cell density and mineralized matrix synthesis during cultivation in rotating bioreactors (26–28). Although the specific mechanism of collision-induced bone tissue synthesis has yet to be elucidated, studies should be carried out to correlate the frequency and intensity of wall collisions with measured outcomes. The mixed scaffolds used in this study can avoid wall collision in rotating bioreactors and thus may improve the environment for cell growth and tissue synthesis. By using the particle-tracking system, we characterized the movement of scaffolds in the rotating bioreactor and estimated the fluid shear. Estimated values of the outer fluid shear lie in the range from 0.16 to 0.32 N/m^2, similar to previous estimates of the physiological level of fluid shear stresses on osteocytes under flow (35).

The rate of glucose consumption by cells plays a major role in determining the adequacy of nutrient supply within scaffolds under static and dynamic culture conditions. The rate of glucose consumption by a single osteoblastic cell was determined by Komarova *et al.* (36). Based on the rate of glucose consumption by cells and the geometry of the scaffolds, we recently developed a model for estimating the adequacy of nutrient supply in the interior of the scaffolds (31). The results from our model indicated that the internal perfusion rate within the pores of the scaffolds was one tenth that of the outer-flow rate, and the minimum internal perfusion rate that was necessary to maintain sufficient glucose supply for osteoblastic cells through the construct thickness of 2.5 mm as used in this study was ≈0.37 mm/s

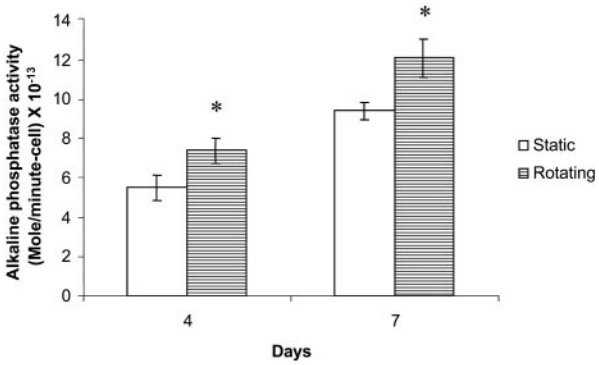

Fig. 4. Alkaline phosphatase activity for cell differentiation. *, A statistically significant, higher ($P < 0.05$) alkaline phosphatase activity than that at static culture conditions. At least three samples from each group were analyzed. Error bars denote standard deviation.

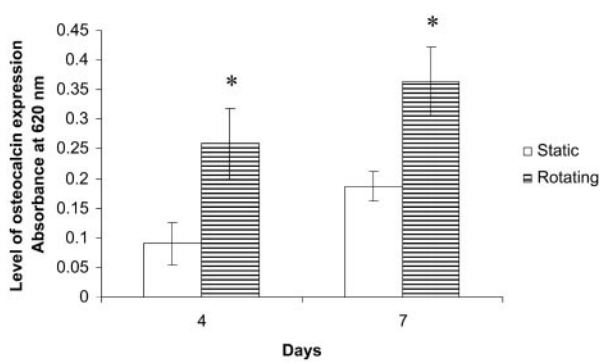

Fig. 6. Graph plot showing relative osteocalcin levels of rat calvarial cells in static and rotating bioreactors at days 4 and 7. *, A statistically significant higher ($P < 0.05$) osteocalcin level than that at static culture conditions. Error bars denote standard deviation.

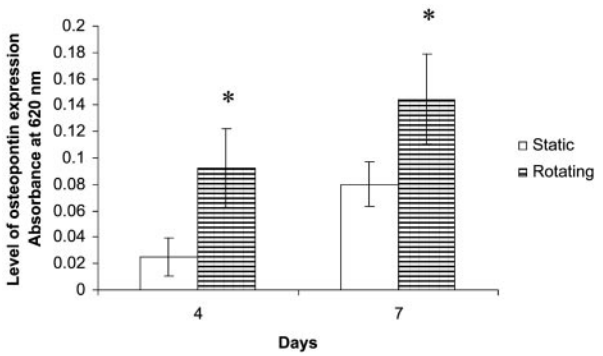

Fig. 7. Graph plot showing osteopontin levels of rat calvarial cells in static and rotating bioreactors at days 4 and 7. *, A statistically significant higher ($P < 0.05$) osteopontin level than that at static culture conditions. Error bars denote standard deviation.

(31). The exterior flow rates of the mixed scaffolds used in this study ranged from 49 to 103 mm/s (Fig. 1*B*), and thus the internal perfusion rates of the scaffolds used in this study are estimated in the range from 4.9 to 10.3 mm/s. These internal perfusion rates are much higher than the minimum internal perfusion rate needed to maintain sufficient glucose supply for osteoblastic cells within the construct thickness of 2.5 mm as determined by our model (31). Therefore, we surmise that sufficient internal perfusion and nutrient flux for cells on these scaffolds can occur by using rotating bioreactors.

In this study, we compared the effects of dynamic flow and static culture conditions on osteoblastic cells by using one composition of mixed 3D scaffolds (HTW and LTW microspheres in a ratio of 60:40). As shown in Fig. 1, this mixed 3D scaffold provides favorable motion trajectories for cells in rotating bioreactors by avoiding wall collision, and the fluid shear of this mixed scaffold in rotating bioreactors is within the physiological range for bone cells (30, 35). In addition, by using the similar level of fluid flow in rotating bioreactors, we have demonstrated that differentiation and mineralization of human Saos-2 cells are significantly enhanced (30).

No significant difference for cell proliferation was observed between static and dynamic flow culture conditions. However, more cells and cellular connections existed in the interior of the scaffolds under dynamic culture conditions than those under static controls (Fig. 2 *C* and *D*). The dynamic flow may improve nutrient supply and increase metabolic waste removal for the cells in the scaffolds and thus promote the cell growth in the interior of the scaffolds in the rotating bioreactors. Under static conditions, nutrient transport and waste-product efflux may be insufficient to maintain cell viability in the interior of the scaffolds. When comparing the surface with the interior of the scaffolds under dynamic flow cultures (Fig. 2 *B* and *D*), more uniformly distributed cellular connections existed in the interior of the scaffolds. These observations indicated that although the outer-flow shear stress was in the physiological level and might not disrupt the attachment of cells on the surface of the scaffolds, it might be strong enough to break down or prevent the formation of some of the cellular connections. On the other hand, the relatively weak internal-flow shear stress (one tenth less than that of the outer-flow shear stress) could provide sufficient internal perfusion and nutrient flux without disturbing the formation of cellular interconnections in the interior of the scaffolds.

Recent studies by our laboratory have shown that enhanced nutrient flux conditions within the microsphere-based scaffolds is favorable for cell growth (30, 31). However, significant differences in total cell numbers in static and dynamic conditions were not detected, likely because of robust cell growth on the exterior surface of statically cultured scaffolds. The phenomenon of comparatively high exterior cell density in static culture is consistent with previous observations of culturing human osteoblast-like cells on microcarrier scaffolds (30) and is generally consistent with prior calculations of nutrient inadequacy in the scaffold interior (31). Moreover, because cell growth and differentiation in osteoblastic cells is known to be reciprocal (37), it is also possible that differences in cell growth under static and dynamic culture conditions are obscured by the enhanced differentiation and correspondingly slower growth of cells in dynamic culture.

Alkaline phosphatase activity and expressions of the proteins, osteocalcin and octeopontin, were significantly increased in rotating bioreactors as compared with those in static controls, indicating that the phenotypic expression of osteoblasts under rotating conditions was enhanced. As indicated by calcium deposition, the matrix synthesis in rotating bioreactors was also significantly increased as compared with that in static controls. Studies using 2D cultures have shown that the expressions of alkaline phosphatase, osteocalcin, and osteopontin in osteoblastic cells started at day 7, and the matrix synthesis of osteoblastic cells started at day 14 (37). Our study showed that the expressions of osteocalcin and osteopontin and matrix synthesis started at an earlier stage (day 4) under dynamic flow conditions, indicating that dynamic flow conditions may cause stimulation of osteoblastic cell function in rotating bioreactors.

We have previously demonstrated that human Saos-2 cells were very sparse in the interior of the scaffolds under static conditions, but they existed extensively in the interior of scaffolds under dynamic flow culture conditions (30). In addition, the differentiation and mineralization of human Saos-2 cells were significantly enhanced under dynamic flow conditions as compared with static cultures after 4 and 7 days in the rotating bioreactors (30). These Saos-2 cell results are consistent with our current study with primary rat calvarial cells. The use of primary calvarial cells is more relevant for applications in tissue-engineered constructs in rotating bioreactors. These cells, as compared with Saos-2 cell lines, have properties closer to the *in vivo* cells and thus might be more indicative of further *in vivo* studies.

The effect of hydrodynamic flow on bone cell response is significant. The dynamic flow environment of the scaffolds improves the supply of nutrients and metabolic product efflux for the cells in the scaffolds and thus maintains cell viability in the interior of the scaffolds and promotes cell differentiation and mineralization in rotating bioreactors. For comparison, longer term (21-day) studies should be performed.

Traditional methods of bone tissue engineering have used both osteoblasts or osteoprogenitor cells isolated from the donor with 3D scaffolds that support tissue growth and mineralized osteoid formation (13–17). The resulting cell-material constructs provide mechanical support and the necessary osteoconductive/inductive and angiogenic interactions at the site of bony repair (13–17). Current studies should focus on the development of dynamic culture system in bioreactors as a enabling technology to provide appropriate balanced levels of nutrient flux that are necessary for large-construct cultivation and to enhance the rate and extent of bone matrix production within the scaffolds. In addition, based on previous reports by our laboratory, the mechanical properties of these scaffolds are in the middle range of human trabecular bone in terms of compressive modulus and compressive strength (32). As a result, these methods of bioreactor-based tissue engineering may reduce the time necessary to engineer clinically relevant quantities of tissue-engineered bone, an issue of considerable clinical and scientific importance.

Conclusions

These studies suggest that the motion trajectories and therefore the flow velocity around and through the scaffolds in rotating bioreactors can be manipulated by varying the ratio of HTW to LTW microspheres. The 3D dynamic flow environment affects bone cell distribution in 3D cultures and enhances osteoblastic cell phenotypic expression and mineralized matrix synthesis within tissue-engineered constructs. The expression of selected bone marker proteins, such as osteocalcin and osteopontin, were also enhanced under the 3D dynamic flow environment. These studies may aid in the design and optimization of 3D scaffolds suitable for bioreactor-based tissue engineering of bone.

This work was supported by National Science Foundation Grants BES0115404, BES0201923, BES0343620, and EEC-9980298 (to C.T.L.), National Aeronautics and Space Administration Grant NAG9-832 (to E.M.L.), National Institutes of Health Training Grant AR07132-23 (to E.A.B.), and the Commonwealth Universal Research Enhancement Program, Pennsylvania Department of Health. C.T.L. was previously the recipient of a Presidential Faculty Fellow Award from the National Science Foundation.

1. Langer, R. & Vacanti, J. P. (1993) *Science* **260,** 920–926.
2. Langer, R., Vacanti, J. P., Vacanti, C., Atala, A., Freed, L. E. & Vunjak-Novakovic, G. (1995) *Tissue Eng.* **1,** 151–161.
3. Bauer, T. W. & Muschler, G. F. (2000) *Clin. Orthop.* **371,** 10–27.
4. Hill, N .M., Horne, J. G. & Devane, P. A. (1999) *Aust. N. Z. J. Surg.* **69,** 726–728.
5. Seiler, J .G. & Johnson, J. (2000) *J. South. Orthop. Assoc.* **9,** 91–97.
6. Mendenhall, S. (2000) in *Bone Engineering*, ed. Davis, J. E. (em squared incorporated, Toronto), pp. 585–590.
7. Jarcho, M. (1981) *Clin. Orthop.* **157,** 259–278.
8. Schmitz, J. P., Hollinger, J. O. & Milam, S. B. (1999) *J. Oral Maxillofac. Surg.* **57,** 1122–1126.
9. Yuasa, T., Miyamoto, Y., Ishikawa, K., Takechi, M., Nagayama, M. & Suzuki, K. (2001) *J. Biomed. Mater. Res.* **54,** 344–350.
10. Yuan, H., Kurashina, K., de Brujin, J. D., Li, Y., de Groot, K. & Zhang, X. (1999) *Biomaterials* **20,** 1799–1806.
11. Freed, L. E., Hollander, A. P., Martin, I., Barry, J. R., Langer, R. & Vunjak-Novakovic, G. (1998) *Exp. Cell Res.* **240,** 58–65.
12. Casser-Bette, M., Murry, A. B., Closs, E. I., Erfle, V. & Schmidit, J. (1990) *Calcif. Tissue Int.* **46,** 46–56.
13. el-Ghannam, A., Ducheyne, P. & Shapiro, I.M. (1995) *J. Biomed. Mater. Res.* **29,** 359–370.
14. Ishaug, S. L., Crane, G. M., Miller, M. J., Yasko, A. W., Yaszemski, M. J. & Mikos, A. G. (1997) *J. Biomed. Mater. Res.* **36,** 17–28.
15. Ishaug-Riley, S L., Crane-Kruger, G. M., Yaszemski, M. J. & Mikos, A. G. (1998) *Biomaterials* **19,** 1405–1412.
16. Devin, J., Attawia, M. A. & Laurencin, C. T. (1996) *J. Biomater. Sci. Polym. Ed.* **7,** 661–669.
17. Laurencin, C. T., Attawia, M. A., Elgendy, H. E. & Herbert, K. M. (1996) *Bone* **19,** S93–S99.
18. Eiselt, P., Kim, B. S., Chacko, B., Isenberg, B., Peters, M. C., Greene, K. G., Roland, W. D., Loebsack, A. B., Burg, K. J., Culberson, C., *et al.* (1998) *Biotechnol. Prog.* **14,** 134–140.
19. Granet, C., Laroche, N., Vico, L., Alexandre, C. & Lafage-Proust, M. H. (1998) *Med. Biol. Eng. Comput.* **36,** 513–519.
20. Klement, B. J. & Spooner, B. S. (1993) *J. Cell. Biochem.* **51,** 252–256.
21. Molnar, G., Schroedl, N. A., Gonda, S. R. & Hartzell, C. R. (1997) *In Vitro Cell. Dev. Biol. Anim.* **33,** 386–391.
22. Becker, J. L. (1993) *J. Cell. Biochem.* **51,** 283–289.
23. Prewett, T. L., Goodwin, T. J. & Spaulding, G. F. (1993) *J. Tissue Cult. Methods* **15,** 29–36.
24. Qiu, Q., Ducheyne, P., Gao, H. & Ayyaswamy, P. (1998) *Tissue Eng.* **4,** 19–34.
25. Lewis, M. L., Moriarity, D. M. & Campbell, P. S. (1993) *J. Cell. Biochem.* **51,** 265–273.
26. Sikavitsas, V. I., Bancroft, G. N. & Mikos, A. G. (2002) *J. Biomed. Mater. Res.* **62,** 136–148.
27. Goldstein, A. S., Juarez, T. M., Helmke, C. D., Gustin, M. C. & Mikos, A. G. (2001) *Biomaterials* **22,** 1279–1288.
28. Cherry, R. S. & Papoutsakis, E. T. (1988) *Biotechnol. Bioeng.* **32,** 1001–1014.
29. Nollert, M. U., Diamond, S. L. & McIntire, L. V. (1991) *Biotechnol. Bioeng.* **38,** 588–602.
30. Botchwey, E. A., Pollack, S. R., Levine, E. M. & Laurencin, C. T. (2001) *J. Biomed. Mater. Res.* **55,** 242–253.
31. Botchwey, E. A., Dupree, M. A., Pollack, S R., Levine, E. M. & Laurencin, C. T. (2003) *J. Biomed. Mater. Res.* **67A,** 357–367.
32. Borden, M. D., Khan, Y., Attawia, M. & Laurencin, C. T. (2002) *Biomaterials* **23,** 551–559.
33. Pollack, S. R., Meaney, D. F., Levine, E. M., Litt, M. & Johnston, E. D. (2000) *Tissue Eng.* **6,** 519–530.
34. Mosmann T. (1988) *J. Immunol. Methods* **65,** 55–63.
35. Weinbaum, S., Cowin, S. C. & Zeng, Y. (1994) *J. Biomech.* **27,** 339–360.
36. Komarova, S. V., Ataullakhanov, F. I. & Globus, R K. (2000) *Am. J. Physiol. Cell Physiol.* **279,** C1220–C1229.
37. Stein, G.S., Lian, J. & Stein, J. (1996) in *Principles of Bone Biology*, eds. Bilezikian, J. P., Raisz, L. G. & Rodan, G. A. (Academic, San Diego), pp. 69–86.